Reduction of Vibration-Induced Artifacts in Synthetic Aperture Radar Imagery

Qi Wang, *Student Member, IEEE*, Matthew Pepin, *Member, IEEE*, Aleck Wright, Ralf Dunkel, Tom Atwood, Balu Santhanam, *Senior Member, IEEE*, Walter Gerstle, Armin W. Doerry, and Majeed M. Hayat, *Senior Member, IEEE*

***Abstract*—Target vibrations introduce nonstationary phase modulation, which is termed the micro-Doppler effect, into returned synthetic aperture radar (SAR) signals. This causes artifacts, or ghost targets, which appear near vibrating targets in reconstructed SAR images. Recently, a vibration estimation method based on the discrete fractional Fourier transform (DFrFT) has been developed. This method is capable of estimating the instantaneous vibration accelerations and vibration frequencies. In this paper, a deghosting method for vibrating targets in SAR images is proposed. For single-component vibrations, this method first exploits the estimation results provided by the DFrFT-based vibration estimation method to reconstruct the instantaneous vibration displacements. A reference signal, whose phase is modulated by the estimated vibration displacements, is then synthesized to compensate for the vibration-induced phase modulation in returned SAR signals before forming the SAR image. The performance of the proposed method with respect to the signal-to-noise and signal-to-clutter ratios is analyzed using simulations. Experimental results using the Lynx SAR system show a substantial reduction in ghosting caused by a 1.5-cm 0.8-Hz target vibration in a true SAR image.**

***Index Terms*—Fractional Fourier transform (FrFT), ghost target, image deghosting, synthetic aperture radar (SAR), vibrating target.**

I. Introduction

SYNTHETIC aperture radar (SAR) is a remote-sensing technique that has been well established over the past few decades [1]–[3]. SAR is capable of generating high-resolution terrain images in all weather conditions, providing complementary and useful information for remote sensing. SAR transmits electromagnetic (EM) radiation to ground scenes and measures their EM reflectivity. This active illumination feature facilitates identification and classification of ground objects.

Inherent in SAR is the assumption that all the targets are static during the data collection process. The returned SAR signals from static targets (after preprocessing) are all stationary, i.e., they are a superposition of pure sinusoids. Conventional SAR image formation methods, which are based on the Fourier transform (FT), are able to focus the targets on their correct positions by "compressing" the returned SAR signals to impulses located at the frequencies that are linearly related to the target's locations. However, SAR is sensitive to low-level target vibrations [4]–[11]. Specifically, target vibrations cause SAR images to contain localized artifacts, or "ghost targets," in the azimuth (cross-range) direction. This is because the vibrations introduce nonstationary phase modulation, which is termed the micro-Doppler effect [8], into the returned SAR signals. The conventional SAR formation methods cannot "compress" nonstationary signals into narrow impulses. Instead, they produce side lobes that appear as the ghost targets. Such ghost targets cause ambiguity in target identification and classification. As such, it would be of great benefit to have a reliable method to remove them. In SAR images, the ghost targets appear identical as the true targets. Therefore, it is impossible to directly remove the ghost targets from the SAR image, by merely using image processing, without risking the removal of true targets [12]. Prior work with rotational micro-Doppler artifacts in SAR separates nonstationary components in time–frequency space decompositions [13], [14], where the extraction of the ghost targets in the image takes place after SAR image formation [15]–[17]. In this paper, a method is proposed to reduce the vibration-induced ghost targets before forming the SAR images.

The specific signal causing these artifacts, i.e., the modulation of the phase history by vibration, is estimated by assuming a sinusoidal vibration. This circumvents the aforementioned difficulty of identifying the ghost targets from the true targets in SAR images. The proposed method is based on a preestimation of the vibration that causes the ghost targets. The vibration is estimated by using a recently developed method that is based on the discrete fractional FT (DFrFT) [18]–[20]. This vibration estimation method is capable of estimating the instantaneous accelerations and frequencies of the vibration from the returned SAR signals. The method includes three main steps.

Manuscript received July 9, 2012; revised March 3, 2013; accepted May 28, 2013. Date of publication July 9, 2013; date of current version March 3, 2014. This work was supported in part by the U.S. Department of Energy under Award DE-FG52-08NA28782, by the National Science Foundation under Award IIS-0813747, by the National Consortium for Measurement and Signature Intelligence (MASINT) Research, by the Naval Postgraduate School under Contract N00244-11-1-0041, and by Sandia National Laboratories.

Q. Wang, M. Pepin, and M. M. Hayat are with the Center for High Technology Materials and the Department of Electrical and Computer Engineering, The University of New Mexico, Albuquerque, NM 87131 USA (e-mail: qwang@ece.unm.edu; pepinm@ece.unm.edu; hayat@ece.unm.edu).

A. Wright and B. Santhanam are with the Department of Electrical and Computer Engineering, The University of New Mexico, Albuquerque, NM 87131 USA.

R. Dunkel is with General Atomics Aeronautical Systems, Inc., San Diego, CA 92128 USA.

T. Atwood and A. W. Doerry are with Sandia National Laboratories, Albuquerque, NM 87123 USA.

W. Gerstle is with the Department of Civil Engineering, The University of New Mexico, Albuquerque, NM 87106 USA.

Color versions of one or more of the figures in this paper are available online at http://ieeexplore.ieee.org.

Digital Object Identifier 10.1109/TGRS.2013.2269138

Provided that the target exhibits a single-component harmonic vibration, the instantaneous vibration displacements are first reconstructed from the estimated vibration accelerations and frequency. Second, a reference signal whose phase is modulated by the estimated vibration displacements is constructed. Finally, the returned SAR signals are multiplied with this reference signal to reduce the vibration-induced phase modulation, and a SAR image with reduced artifacts is then formed by the conventional SAR image formation methods. The performance of the proposed method with respect to the signal-to-noise ratio (SNR) and the signal-to-clutter ratio (SCR) is analyzed using simulations. In an experiment using the Lynx SAR system [21], the proposed method substantially reduced the ghost targets caused by a 1.5-cm 0.8-Hz vibration in a true SAR image.

The remainder of this paper is organized as follows. In Section II, we provide a detailed model for the vibration-induced phase modulation in returned SAR signals. In Section III, germane aspects of the DFrFT-based vibration estimation method are reviewed, followed by the development of the proposed deghosting method. In Section IV, the performance of the proposed method is analyzed with simulated SAR data. Experimental results are shown in Section V, and the conclusions are given in Section VI.

II. Model

A. Signal Model

In this paper, we assume that the SAR system works in the spotlight mode [2]. For spotlight-mode SAR, the image is usually formed by using the polar format algorithm (PFA) [2]. In the PFA, the returned SAR signals are first demodulated and low-pass filtered. This is followed by polar-to-rectangular resampling, which is applied to the SAR phase history to correct for irregular sample spacing due to the collection geometry. Next, an autofocus method is usually applied to the SAR phase history to improve the quality of the SAR image [2]. The formatted 2-D phase history, assuming a point target model, can be written as

$$r[l,n] \approx \sum_i \sigma_i \exp\left[-j(k_x x_i l + k_y y_i n + \phi_i)\right] + \hat{w}[l,n] \quad (1)$$

where (x_i, y_i) and (σ_i, ϕ_i) are the coordinates and the complex reflectivity of the ith target, respectively. The noise is represented by $\hat{w}[l,n]$. The indices (l,n) correspond to the range and azimuth directions, respectively; they are constrained by $0 \le l < L$ and $0 \le n < N$, where L is determined by the size of the synthetic aperture, and N is determined by the bandwidth of the sent pulse [2]. The scaling parameters (k_x, k_y) are

$$k_x = \frac{4\pi K}{c f_s} \quad k_y \approx \frac{4\pi f_c V}{c R_0 f_{\mathrm{prf}}} \quad (2)$$

where K is the chirp rate of the sent pulse, c is the propagation speed of the sent pulse, f_s is the sampling frequency of the returned SAR signal, f_c is the carrier frequency of the sent pulse, V is the speed of the antenna carrier, R_0 is the distance from the scene center to the midaperture, and f_{prf} is the pulse-repetition frequency (PRF).

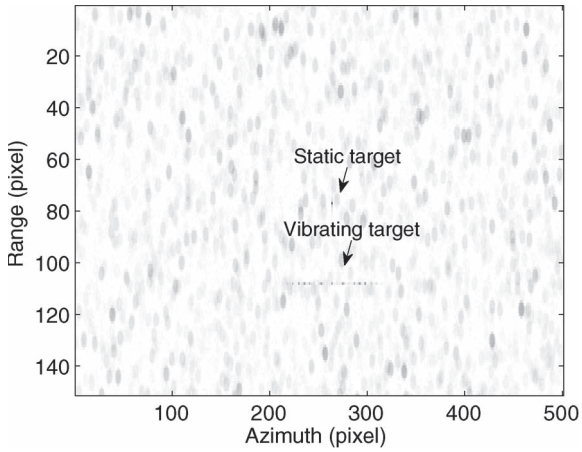

Fig. 1. Synthesized SAR image containing a static target and a vibrating target. The pixel size is 0.33 m × 0.33 m, and the SNR and SCR are both 15 dB. The vibration is a single-component oscillation of 2 Hz with an amplitude of 1 cm. The vibration-induced ghost targets appear near the vibrating target along the azimuth direction.

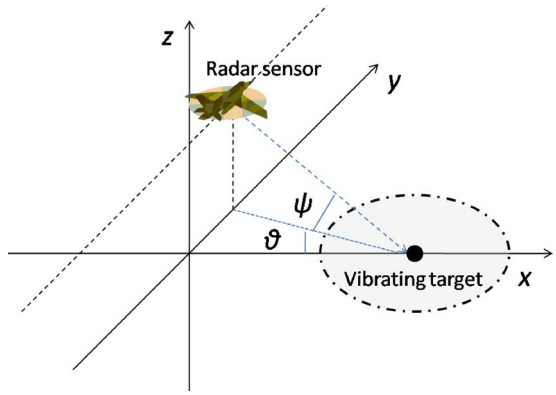

Fig. 2. Three-dimensional SAR data collection geometry. In spotlight-mode SAR, the antenna always points to the center of the scene during the data collection process.

B. Model for Vibrating Targets

SAR assumes that all ground targets are static. The SAR image is formed by applying a 2-D FT to $r[l,n]$ in (1). When nonstatic targets are present in the scene, however, the FT-based image formation techniques cannot focus nonstatic targets, and ghost targets appear in the reconstructed SAR image [4]–[8]. Fig. 1 shows a synthesized SAR image containing a static target and a vibrating target. The pixel size is 0.33 m in both directions. The SNR and SCR are both 15 dB. The vibration is a single-component oscillation of 2 Hz with an amplitude of 1 cm. As shown in the figure, the vibration causes several ghost targets around the vibrating target in the azimuth direction.

The signal model described in (1) can be extended to vibrating targets. Fig. 2 shows a 3-D SAR flight geometry, with a vibrating target located at the origin. At a given time, the radar sensor locates at polar angles ψ and θ to the target. Provided that the squint angle θ is small and the vibration amplitude (usually several millimeters) is much smaller than the line-of-sight distance from the radar sensor to the ground scene, the

formatted returned signal $r[l,n]$ containing vibration targets can be written as [2], [5], [18]

$$r[l,n] \approx \sum_i \sigma_i \exp\left[-j(k_x \bar{x}_i l + k_y \bar{y}_i n + k_v \Delta x_i[n] + \phi_i)\right] + \hat{w}[l,n] \quad (3)$$

where $k_v = 4\pi f_c/c$, and $\Delta x_i[n]$ is the vibration displacement of the ith target in the range direction. The coordinates $(\bar{x}_i, \bar{y}_i)$ are used to denote the average position of the vibrating target during the data collection process. Clearly, it is mainly the range component of the vibration displacement that introduces phase modulation into the SAR phase history.

If we apply the FT to $r[l,n]$ in the range direction, we obtain the so-called range-compressed signal $\hat{s}[x;n]$, where x denotes the range position. After the range compression, the vibrating target is usually focused at a given range location (note that the ghost targets appear only in the azimuth direction). If we assume that there is no more than one vibrating target at a given range location x^*, then $\hat{s}[x^*;n]$ can be written as

$$\hat{s}[x^*;n] \doteq s[n] \approx \sigma A_x \exp\left[-j(k_y \bar{y} n + k_v \Delta x[n] + \phi)\right] + c[n] + w[n] \quad (4)$$

where A_x is a complex scaling factor generated by range compression. We define $s[n]$ as the signal of interest (SoI). The only signal explicitly written is that from the vibrating target. Signals from other static targets at the same range locations are collectively represented by $c[n]$. Conventionally, $c[n]$ is referred to as the "clutter signal" or, simply, "clutter."

The SCR used in our analysis is defined with respect to reconstructed SAR images as

$$\text{SCR} = 20 \log \frac{|\sigma_v|}{|\sigma_c|} \quad (5)$$

where σ_v is the reflectance of the vibrating target, and σ_c is the average reflectance of 1 m^2 of clutter. We assume that the reflectance of the clutter pixel is Gamma distributed with the shape parameter $k_{\text{gam}} = \sigma_c$ (the scale parameter is always set to be 1) [22]. A circle-shaped averaging filter with a radius of 1 m is applied to the clutter to simulate the correlations in neighbor pixels [22]. The SNR is defined with respect to the returned SAR signals as

$$\text{SNR} = 10 \log \frac{E_s}{E_w} \quad (6)$$

where E_s is the energy of the signal (including both vibrating targets and clutter), and E_w is the energy of the noise. We assume that the noise is white and Gaussian.

III. Method Development

For its key role in the process of reducing the vibration-induced artifacts, we first review the DFrFT-based vibration estimation method, freely drawing from the literature [18]. The deghosting method is then developed.

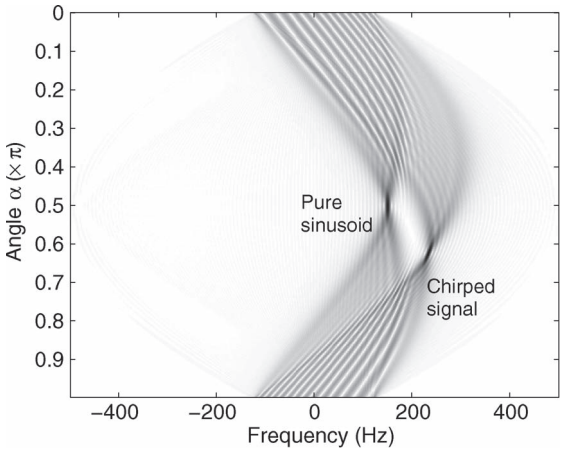

Fig. 3. Demonstration of the angle–frequency plane by calculating the DFrFT of a signal containing a sinusoidal signal and a chirped signal.

A. Review of the DFrFT-Based Vibration Estimation Method

Recently, a time–frequency method based on the DFrFT has been proposed to estimate low-level target vibrations in returned SAR signals. Simulations and experimental results show that this method is capable of estimating low-level vibrations (e.g., 1.5-mm amplitude and 5 Hz) with both practical SNR and SCR. For completeness, a brief introduction of this method is provided here. The reader may find more details in [18], [20], and [23]–[25].

The DFrFT is an analysis tool specifically geared toward chirp signals [26]–[29]. By introducing a new angular parameter α, the DFrFT is able to estimate the chirp rate of a chirp signal. By applying the DFrFT, a chirp signal is transformed into a 2-D impulse in the angle–frequency plane, the location of which is determined from the center frequency and the chirp rate of the signal. For instance, Fig. 3 shows the DFrFT of a two-component signal containing a chirp signal with a chirp rate of 400 Hz/s at a center frequency of 250 Hz and, for reference and comparison, a pure sinusoid with a frequency of 150 Hz. The frequency axis displayed is the same as that used for the discrete FT (DFT). The angle α ranges from $-\pi$ to π. For $\alpha = \pi/2$, the DFrFT coincides with the DFT. The peak corresponding to the sinusoid component locates on the $\alpha = \pi/2$ line, which indicates that the sinusoid component has a zero chirp rate. On the other hand, the deviation from the peak corresponding to the chirp component to the $\alpha = \pi/2$ line is used to calculate the chirp rate, and there is one-to-one mapping between the deviation and the chirp rate under certain conditions [24], [25].

Following [18], we apply the DFrFT-based vibration estimation method to the SoI defined in (4). In a short time window starting at m, a second-order approximation can be applied to the vibration displacement $\Delta x[n]$, and the SoI in (4) becomes

$$s[n] \approx \sigma \exp\left[j\left(\phi - \frac{4\pi f_c}{c}\Delta x[m] + \left(k_y \bar{y} - \frac{4\pi f_c v[m]}{c f_{\text{prf}}}\right) n - \frac{2\pi f_c a[m]}{c f_{\text{prf}}^2} n^2\right)\right] + c[n] + w[n], m \le n < m + N_w \quad (7)$$

where $v[m]$ and $a[m]$ are the instantaneous vibration velocity and the instantaneous vibration acceleration, respectively; and N_w is the size of the window. According to (7), $x[n]$ in a short time window is approximately a chirp signal, and its chirp rate is proportional to the instantaneous vibration acceleration $a[m]$. Once the chirp rate is estimated by the DFrFT, the estimated vibration acceleration is calculated via

$$\hat{a}[m] = -\frac{cf_{\text{prf}}^2}{2\pi f_c}\hat{c}_r[m] \tag{8}$$

where $\hat{c}_r[m]$ is the estimated chirp rate. By estimating the chirp rates of $x[n]$ in successive sliding short time windows, the instantaneous vibration acceleration is tracked. As a result, the history of the instantaneous vibration accelerations is reconstructed, and the vibration frequency $\hat{f}_v$ can be estimated from the spectrum of sequence of the estimated instantaneous accelerations of the vibration. Details of this DFrFT-based vibration estimation method are provided in [18].

B. Deghosting Method

In this paper, we focus on reducing the artifacts caused by single-component vibrations that are common in real-world applications [5], [8], [18]. Thus, the instantaneous vibration displacements can be written as

$$\Delta x(t) = A_v \sin(2\pi f_v t + \phi_v) \tag{9}$$

where A_v is the vibration amplitude, f_v is the vibrating frequency, and ϕ_v is the initial phase. The second derivative of Δx yields the instantaneous vibration acceleration

$$a_v(t) = (\Delta x(t))'' = -4\pi^2 f_v^2 A_v \sin(2\pi f_v t + \phi_v). \tag{10}$$

As such, we can estimate the instantaneous vibration displacements from the estimated instantaneous vibration acceleration via

$$\Delta\hat{x}[n] = -\frac{1}{4\pi^2 \hat{f}_v^2}\hat{a}[n] \tag{11}$$

where $\hat{f}_v$ and $\hat{a}[n]$ are the estimated vibrating frequency and the estimated instantaneous vibration accelerations using the aforementioned DFrFT-based vibration estimation method. A reference signal $g[n]$ is then reconstructed from $\Delta\hat{x}[n]$ as

$$g[n] = \exp\left[jk_v\Delta\hat{x}[n]\right]. \tag{12}$$

In the ideal case where no clutter and noise are present, we simply multiply (demodulate) the SoI with the reference signal $g[n]$ and obtain

$$\begin{aligned}\bar{s}[n] &= \sigma \exp\left[-j\left(k_y\bar{y}n + k_v\left(\Delta\hat{x}[n] - \Delta x[n]\right)\right) + \phi\right)] &(13)\\ &\approx \sigma \exp\left[-j(k_y\bar{y}n + \phi)\right]. &(14)\end{aligned}$$

Provided that the estimated vibration displacement is accurate, the vibration-induced phase modulation can be substantially reduced because the vibration-induced phase modulation is now removed from the SoI. Therefore, the FT-based conventional SAR image formation methods can focus the vibrating target at its correct azimuth position $\bar{y}$.

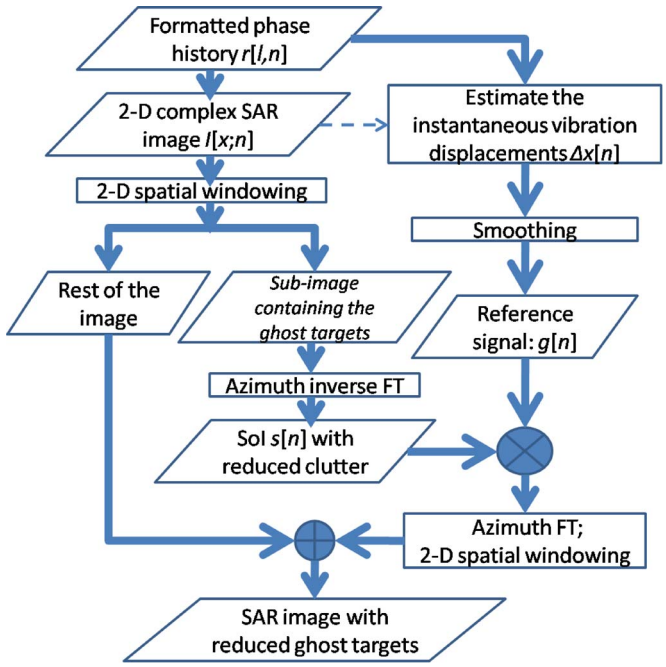

Fig. 4. Flowchart of the proposed deghosting method. The skewed rectangles represent data, and the rectangles represent operations.

TABLE I
SAR SYSTEM PARAMETERS USED IN THE SIMULATION

parameter	quantity
pixel dimension	0.33×0.33 m^2
nominal slant-range	10000 m
nominal grazing angle	10°
carrier frequency	$f_c = 16$ GHz
sent pulse bandwidth	$f_0 = 500$ MHz
plane velocity	$V = 200$ m/s
pulse repetition frequency	720 Hz

In real-world applications, however, the presence of clutter and noise is inevitable. In this case, the deghosting process described in (14) is applied to the clutter signal and noise as well, which causes an unwanted side effect in the SAR image. To overcome this side effect, preprocessing is applied to the returned SAR signals before applying the multiplication in (14). First, we find the rectangular region containing all the ghost targets on the image. The image is visually inspected to confirm the presence of ghost targets along the azimuthal direction. Low-level target vibrations typically do not introduce significant smear in the range direction; therefore, the rectangle usually only spans three to five range lines depending on the size of the target. The cluster of ghost targets and the clutter are seen by plotting the magnitude of the range line where the vibrating target is located. Second, the thresholding technique proposed in [30] is used to differentiate the cluster of ghost targets from the clutter. We use the maximum intensity in the cluster as the reference intensity, and we set the boundary of the rectangle at the pixel cell that is smaller than a thresholding ratio of the reference intensity. According to our experience, a proper threshold ratio is from 0.2 to 0.3. As such, the subimage containing the ghost targets is cropped out from the image by using a 2-D spatial window. Third, the inverse FT is applied to the subimage in the azimuth direction to form the SoIs with reduced clutter and noise. The deghosting method is applied

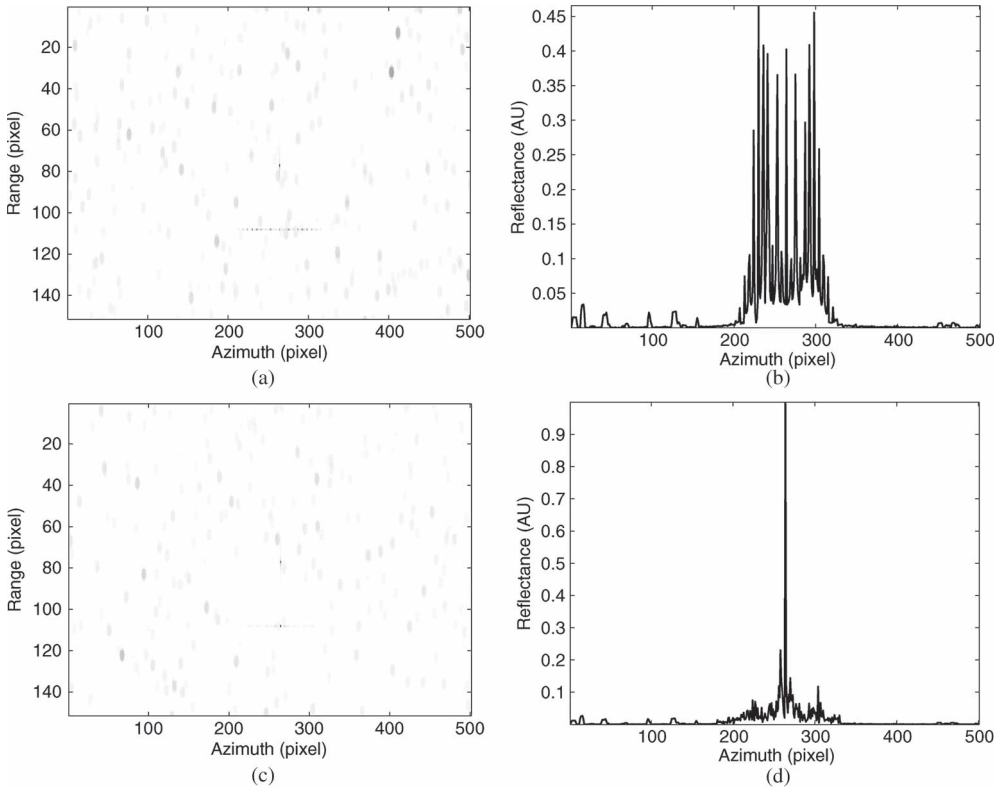

Fig. 5. Synthesized SAR images with both SNR and SCR of 30 dB. The vibration is a 4-Hz oscillation with an amplitude of 1 cm. The proposed algorithm substantially reduced the vibration-induced artifacts. (a) Synthesized SAR image containing one (middle) static target and one (bottom) vibrating target. (b) Magnitude of range line #107 of the SAR image [see Fig. 5(a)], where the vibrating target was located. (c) Deghosted SAR image after applying the proposed method. (d) Magnitude of range line #107 of the deghosted SAR image [see Fig. 5(c)], where the vibrating target was located.

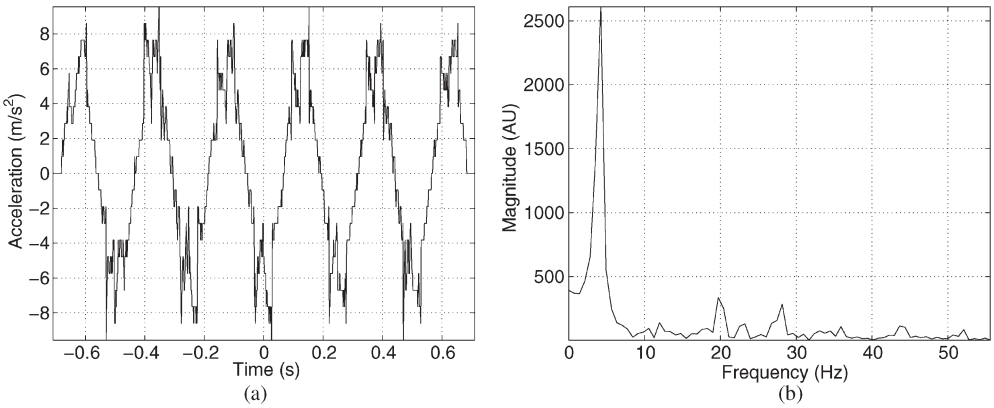

Fig. 6. Estimated instantaneous vibration accelerations and spectrum by using the DFrFT-based vibration estimation method with both SNR and SCR of 30 dB. The estimated vibration frequency is 4 Hz, which is correct. (a) Estimated instantaneous vibration accelerations. (b) Estimated instantaneous vibration spectrum.

to the filtered SoIs. Finally, the deghosted region is filtered by the same 2-D spatial window again and registered at the known position of the SAR image to form a complete SAR image with reduced ghost targets.

It is also known that the presence of clutter and noise causes performance degradation in the vibration estimation process so that the estimated vibration displacements may be "noisy." In this case, the vibration-induced phase modulation cannot be removed in a definitive manner, and the residual artifacts may be still substantial. To overcome this, a smoothing method is employed to prefilter the estimated vibration displacements. For the simulated examples and the experiment in this paper, we use the simple moving-average method, and it is generally sufficient to avoid substantial residual artifacts. The flowchart of the deghosting method is shown in Fig. 4.

IV. Performance Analysis Using Simulated SAR Data

The proposed deghosting method was first verified by means of simulation. An airborne spotlight-mode SAR working in the K_u band was simulated. Table I lists the key system parameters associated with the simulation. Fig. 5(a) shows a synthesized SAR image containing one static target (above) and one vibrating target (below) with both SNR and SCR of 30 dB. The vibration was a 4-Hz oscillation with an amplitude

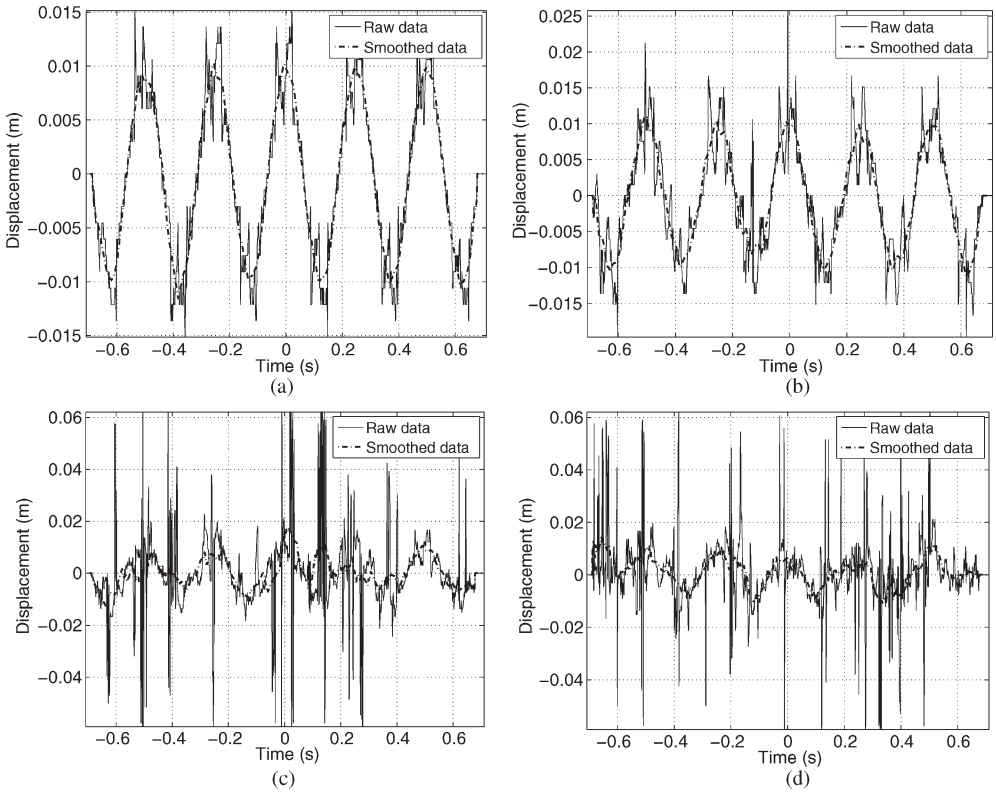

Fig. 7. Estimated instantaneous vibration displacements of a 4-Hz vibration with an amplitude of 1 cm with different SNRs and SCRs. (a) Estimated instantaneous vibration displacements of a 4-Hz vibration with an amplitude of 1 cm with both SNR and SCR of 30 dB. (b) Estimated instantaneous vibration displacements of a 4-Hz vibration with an amplitude of 1 cm, with an SNR of 1 dB and an SCR of 30 dB. (c) Estimated instantaneous vibration displacements of a 4-Hz vibration with an amplitude of 1 cm, with an SNR of −3 dB and an SCR of 30 dB. (d) Estimated instantaneous vibration displacements of a 4-Hz vibration with an amplitude of 1 cm, with an SNR of 30 dB and an SCR of 15 dB.

of 1 cm. As expected, the static target did not exhibit ghosting. For the vibrating target, however, the vibration-induced ghost targets spanned roughly 100 pixels in the azimuth direction. The magnitude of range line #107 of the SAR image, where the vibrating target was located, is shown in Fig. 5(b). It is difficult to find the location of the vibrating target in the cluster of the ghost targets; therefore, it is hard to remove the ghost targets directly from the SAR image without the risk of removing the actual target. The estimated instantaneous vibration accelerations using the DFrFT-based method are shown in Fig. 6(a), and the estimated vibration spectrum is shown in Fig. 6(b). According to the peak location in Fig. 6(b), the estimated vibration frequency was 4.0 Hz. Using this information, the estimated instantaneous vibration displacements were reconstructed, as shown in Fig. 7(a). The moving-average smoothing method was applied to the estimated instantaneous vibration displacements, the result of which is also shown in Fig. 7(a). The SAR image after applying the proposed deghosting method is shown in Fig. 5(c). For a fair comparison, the two SAR images in both Fig. 5(a) and (c) were scaled to the same dynamic range. According to Fig. 5(c), the vibrating target was well focused in the azimuth direction, with only a few dim ghost targets, by using the proposed method. The signal shown in Fig. 5(b) after applying the proposed deghosting method is shown in Fig. 5(d). It showed that the side lobes were significantly reduced.

The performance of the proposed method was analyzed for different SNR and SCR levels by simulations with the same system parameters used above. In general, the proposed method performs well for an SNR down to 0 dB. This is because the noise is white Gaussian noise defined with respect to the returned SAR signals, and the FT-based range-compression process concentrates the energy from the targets but not the noise. Hence, the range compression effectively increases the SNR of the SoI from the returned SAR signals. The SAR image and the magnitude of the corresponding range line #107 with an SNR of 1 dB and an SCR of 30 dB are shown in Fig. 8(a) and (b), respectively. The estimated vibration displacements are shown in Fig. 7(b). The SAR image and the magnitude of the corresponding range line #107 after applying the deghosting method are shown in Fig. 8(c) and (d), respectively. Although these results appeared more "noisy" than those shown in Fig. 5(c) and (d), the ghost targets were still substantially reduced. The SAR image and the magnitude of the corresponding range line #107 with an SNR of −3 dB and an SCR of 30 dB are shown in Fig. 9(a) and (b), respectively. The estimated vibration displacements are shown in Fig. 7(c). The SAR image and the magnitude of the corresponding range line #107 after applying the deghosting method are shown in Fig. 9(c) and (d), respectively. In this case, the proposed method still reduced the ghost targets, but not in a substantial manner.

The performance of the proposed method is strongly affected by the clutter. According to the simulation results, the proposed method can substantially reduce the ghost targets for an SCR down to 18 dB. The signals from the clutter are similar to the ones from the vibrating target. Thus, they interfere with the signals from the vibrating targets, which significantly decreases

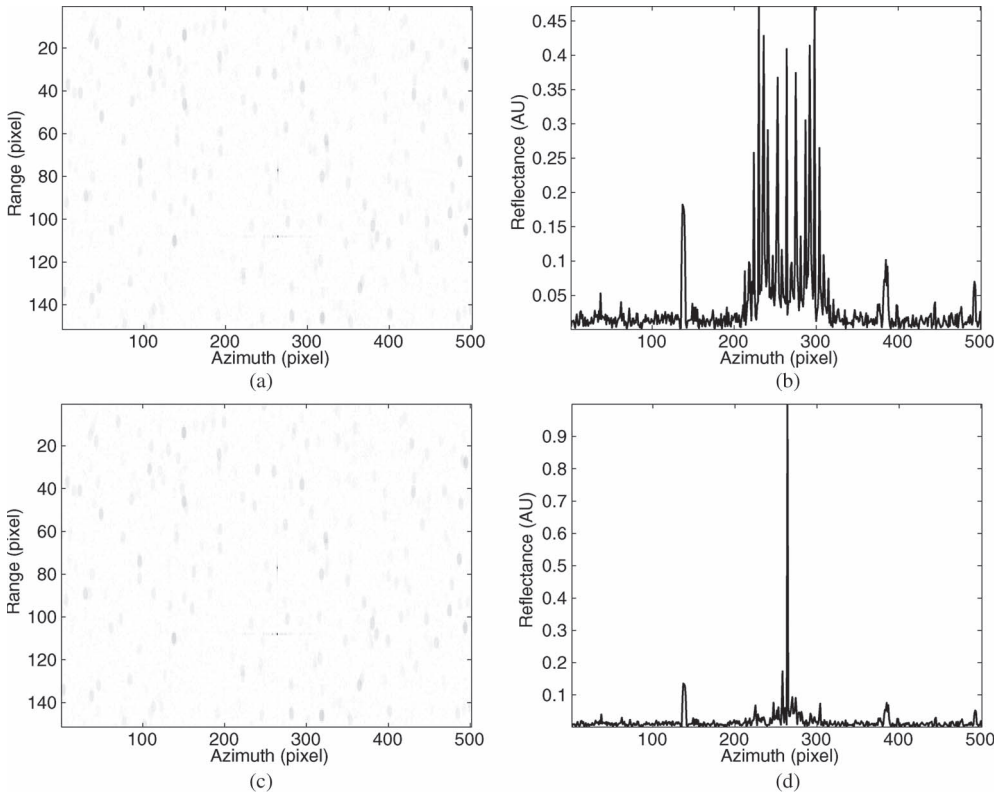

Fig. 8. Deghosted SAR image after applying the proposed method for SNR $= 1$ dB and SCR $= 30$ dB. (a) Synthesized SAR image containing one (middle) static target and one (bottom) vibrating target. (b) Magnitude of range line #107 of the SAR image [see Fig. 8(a)], where the vibrating target was located. (c) Deghosted SAR image after applying the proposed method. (d) Magnitude of range line #107 of the deghosted SAR image [see Fig. 8(c)], where the vibrating target was located.

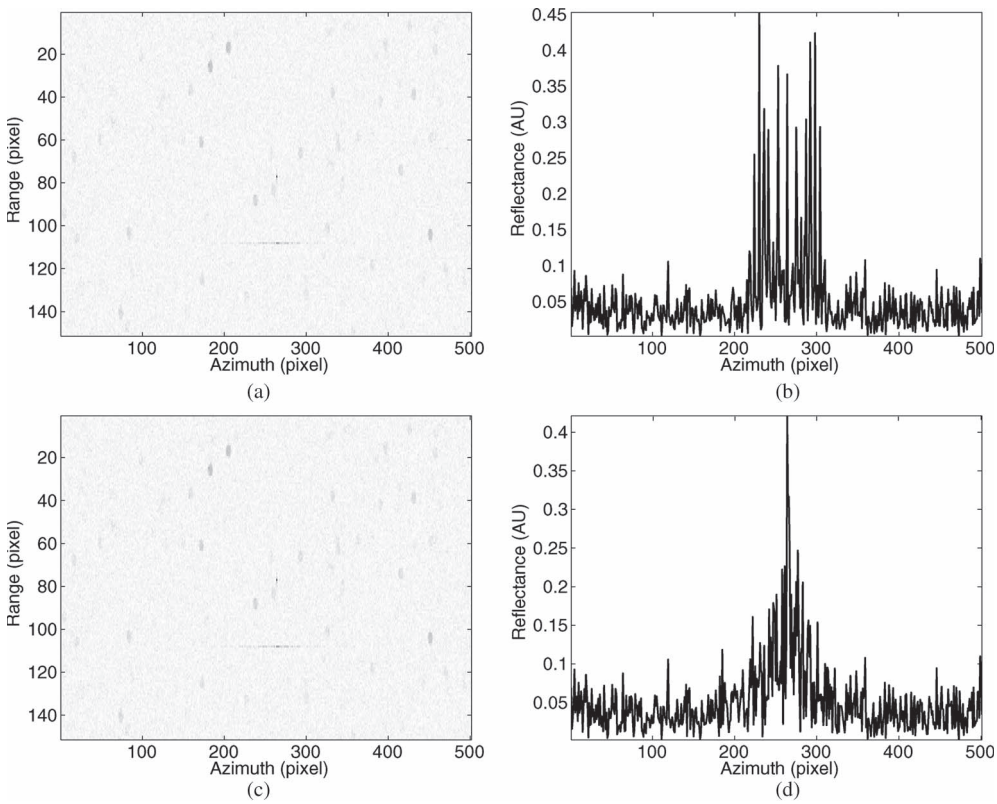

Fig. 9. Deghosted SAR image after applying the proposed method for SNR $= -3$ dB and SCR $= 30$ dB. (a) Synthesized SAR image containing one (middle) static target and one (bottom) vibrating target. (b) Magnitude of range line #107 of the SAR image [see Fig. 9(a)], where the vibrating target was located. (c) Deghosted SAR image after applying the proposed method. (d) Magnitude of range line #107 of the deghosted SAR image [see Fig. 9(c)], where the vibrating target was located.

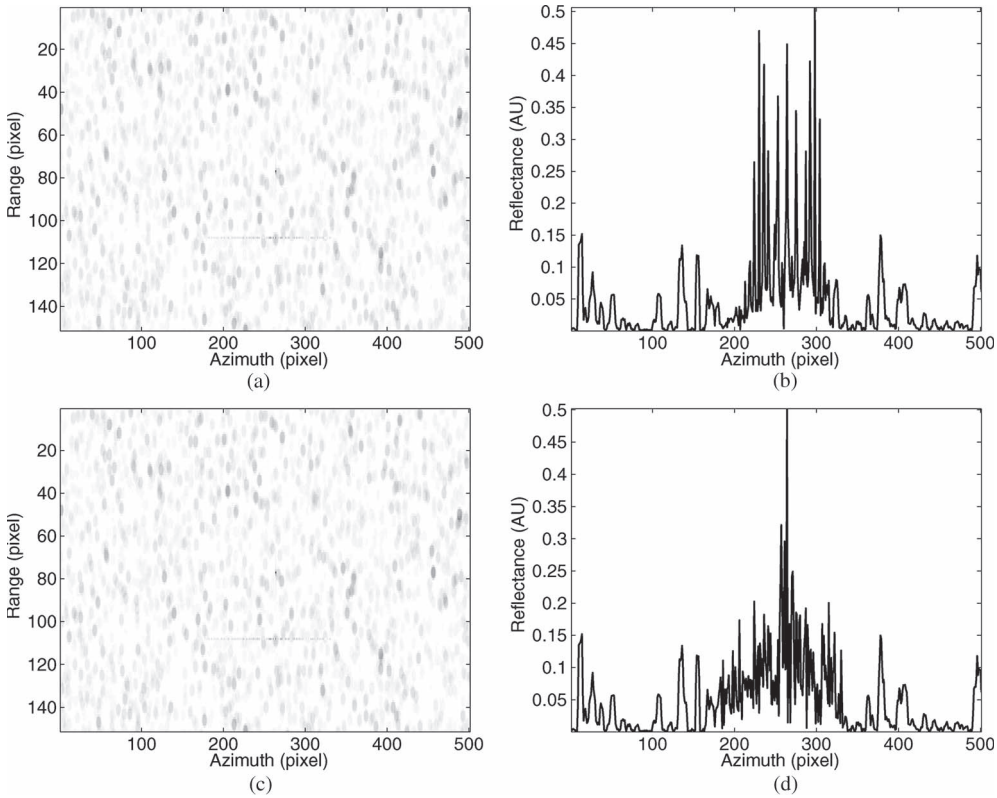

Fig. 10. Deghosted SAR image after applying the proposed method for SNR $= 30$ dB and SCR $= 15$ dB. (a) Synthesized SAR image containing one (middle) static target and one (bottom) vibrating target. (b) Magnitude of range line #107 of the SAR image [see Fig. 10(a)], where the vibrating target was located. (c) Deghosted SAR image after applying the proposed method. (d) Magnitude of range line #107 of the deghosted SAR image [see in Fig. 10(c)], where the vibrating target was located.

TABLE II
SAR SYSTEM PARAMETERS USED IN THE EXPERIMENT

parameter	quantity
pixel dimension	0.25×0.25 m^2
nominal resolution	0.3×0.3 m^2
patch center location	$(0, 9920, -2113)$ m
carrier frequency	$f_c = 16$ GHz, K_u band
length of the synthetic aperture	$L = 333$ m
plane velocity	$V_a = 78$ m/s
pulse repetition frequency	303 Hz

the accuracy in estimating the instantaneous vibration accelerations. This further degrades the performance of the proposed deghosting method. The SAR image and the magnitude of the corresponding range line #107 with an SNR of 30 dB and an SCR of 15 dB are shown in Fig. 10(a) and (b), respectively. The estimated vibration displacements are shown in Fig. 7(d). The SAR image and the reflectance of the corresponding range line after applying the deghosting method are shown in Fig. 10(c) and (d), respectively. In this case, the proposed method only reduced a small portion of the ghost targets.

V. EXPERIMENTAL RESULTS USING THE LYNX SAR SYSTEM

An experiment was conducted in collaboration with General Atomics Aeronautical Systems, Inc. (GA-ASI), San Diego, CA, USA, using the Lynx SAR system [21]. The parameters used in the experiment are listed in Table II. A vibrating retroreflector with a lateral length of 21 in was constructed in our laboratory at The University of New Mexico, Albuquerque, NM, USA, and deployed on the test ground near Julian, CA, USA, as shown in Fig. 11(a). Fig. 12(a) shows the reconstructed SAR image with a nominal resolution of 0.3 m in each direction. The image of the vibrating target was located at the bottom right section of the frame (see magnified inset). It appeared as a sequence of points in the azimuth direction, with the actual object surrounded at each side with a series of ghost targets. The vibration-induced ghost targets spanned about 100 pixels in the azimuth direction. There were also several well-separated static retroreflectors extending from the center of the image to the top right corner; as expected, they did not exhibit any ghosting. The vibration was estimated by first using the DFrFT-based method. Fig. 11(b) shows the estimated instantaneous vibration accelerations for a duration of 3.2 s. The vibrating frequency was estimated to be 0.8 Hz by the peak location in the estimated vibration spectrum shown in Fig. 11(c). The instantaneous vibration displacements and the smoothed version are shown in Fig. 11(d). The moving-average method was used for the smoothing. Fig. 12(b) shows the SAR image after applying the proposed deghosting method to the SAR image in Fig. 12(a). The vibration-induced ghost targets spanned only 20 pixels in the azimuth direction.

VI. CONCLUSION

In this paper, a deghosting method has been proposed for vibrating targets in SAR images. This method employs the DFrFT-based vibration estimation method to first estimate the instantaneous vibration displacements and then reconstructs a

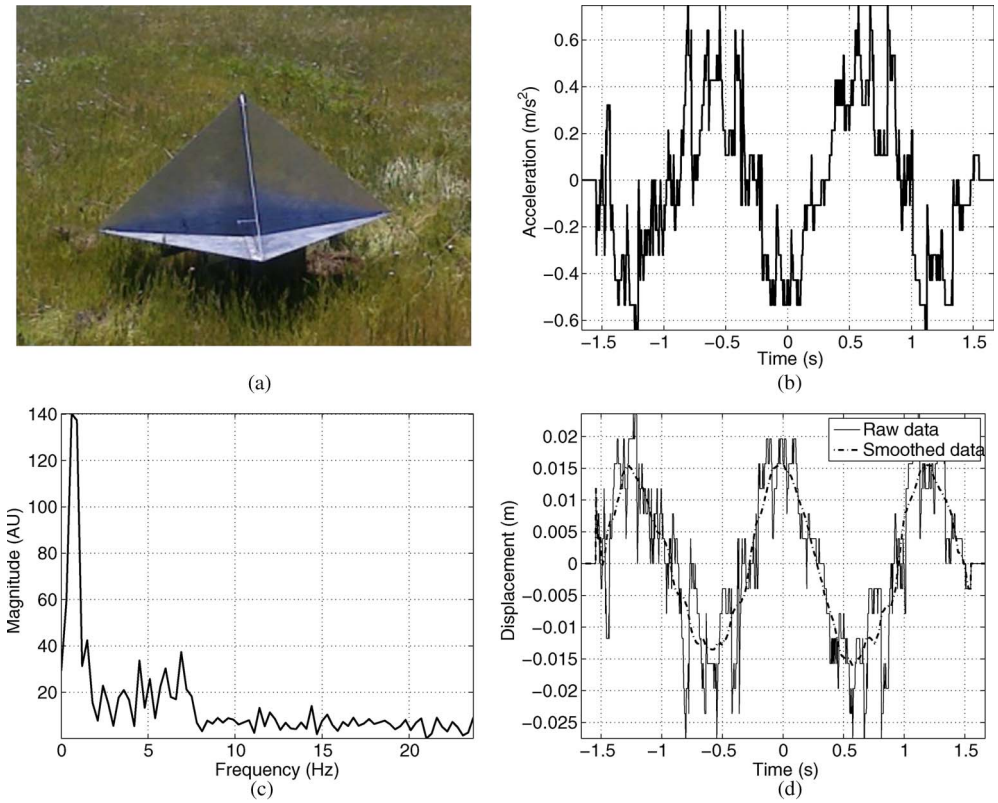

Fig. 11. Vibration target on the test ground and the estimated results of the vibration using the DFrFT-based vibration estimation method. The target was an aluminum triangular trihedral with a lateral length of 21 in fabricated at The University of New Mexico, Albuquerque, NM, USA. The vibration frequency and the amplitude were measured in the laboratory as 0.8 Hz and 1.5 cm, respectively. (a) Vibrating retroreflector on the test ground near Julian, CA, USA. (b) Estimated instantaneous vibration accelerations for 3.2 s using the DFrFT-based vibration estimation method. (c) Spectrum of the estimated instantaneous vibration accelerations. According to the peak location, the vibrating frequency was estimated to be 0.8 Hz. (d) Estimated instantaneous vibration displacements alongside a smoothed version.

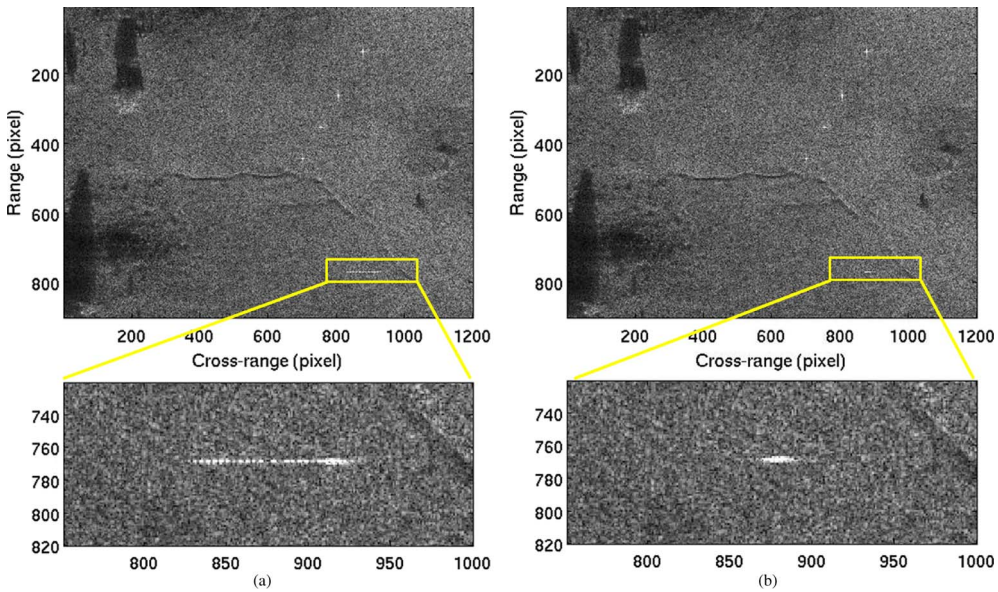

Fig. 12. SAR image provided by the GA-ASI Lynx system. The nominal resolution of the SAR image is 0.3 m in each direction. The vibrating test target is in the lower right portion of this image. Unrelated to this project are a few static targets diagonally extending from the center of the image toward the top right corner. (a) Vibration-induced ghost targets span about 100 pixels in the azimuth direction before applying the proposed method. (b) Vibration-induced ghost targets spanned only 20 pixels in the azimuth direction after applying the proposed method.

reference signal to compensate, before forming the SAR image, for the vibration-induced phase modulation in returned SAR signals before forming the SAR image. The performance of the proposed method was analyzed using simulations. The method was applied to an actual SAR image generated by the Lynx SAR system and substantially reduced the ghost targets caused by a 1.5-cm 0.8-Hz vibration. SAR images with reduced artifacts are helpful in identifying and classifying ground targets,

particularly when used in conjunction with the estimated vibration information.

ACKNOWLEDGMENT

The authors would like to thank GA-ASI for making the Lynx system available to this project.

REFERENCES

[1] I. G. Cumming and F. H. Wong, *Digital Processing of Synthetic Aperture Radar Data: Algorithms and Implementation*. Norwood, MA, USA: Artech House, 2005.
[2] C. V. Jakowatz, D. E. Wahl, P. H. Eichel, D. C. Ghiglia, and P. A. Thompson, *Spotlight-Mode Synthetic Aperture Radar: A Signal Processing Approach*. New York, NY, USA: Springer-Verlag, 1996.
[3] M. Soumekh, *Synthetic Aperture Radar Signal Processing With MATLAB Algorithms*. New York, NY, USA: Wiley, 1999.
[4] R. K. Raney, "Synthetic aperture imaging radar and moving targets," *IEEE Trans. Aerosp. Electron. Syst.*, vol. AES-7, no. 3, pp. 499–505, May 1971.
[5] T. Sparr and B. Krane, "Micro-Doppler analysis of vibrating targets in SAR," *Proc. Inst. Elect. Eng.—Radar, Sonar Navig.*, vol. 150, no. 4, pp. 277–283, Aug. 2003.
[6] M. Rüegg, E. Meier, and D. Nüesch, "Constant motion, acceleration, vibration, and rotation of objects in SAR data," in *Proc. SPIE, SAR Image Anal., Modeling, Tech. VII*, 2005, vol. 5980, pp. 48–59.
[7] M. Rüegg, E. Meier, and D. Nüesch, "Vibration and rotation in millimeter-wave SAR," *IEEE Trans. Geosci. Remote Sens.*, vol. 45, no. 2, pp. 293–304, Feb. 2007.
[8] V. C. Chen, F. Li, S. Ho, and H. Wechsler, "Micro-Doppler effect in radar: Phenomenon, model, and simulation study," *IEEE Trans. Aerosp. Electron. Syst.*, vol. 42, no. 1, pp. 2–21, Jan. 2006.
[9] X. Bai, M. Xing, F. Zhou, G. Lu, and Z. Bao, "Imaging of micromotion targets with rotating parts based on empirical-mode decomposition," *IEEE Trans. Geosci. Remote Sens.*, vol. 46, no. 11, pp. 3514–3523, Nov. 2008.
[10] Q. Wang, M. Xing, G. Lu, and Z. Bao, "High-resolution three-dimensional radar imaging for rapidly spinning target," *IEEE Trans. Geosci. Remote Sens.*, vol. 46, no. 1, pp. 22–30, Jan. 2008.
[11] X. Li, B. Deng, Y. Qin, H. Wang, and Y. Li, "The influence of target micromotion on SAR and GMTI," *IEEE Trans. Geosci. Remote Sens.*, vol. 49, no. 7, pp. 2738–2751, Jul. 2011.
[12] Q. Wang, M. Pepin, R. Dunkel, T. Atwood, A. W. Doerry, B. Santhanam, W. Gerstle, and M. M. Hayat, "Reduction of vibration-induced artifacts in synthetic-aperture-radar imagery using the fractional Fourier transform," in *Proc. IEEE ICIP*, Orlando, FL, USA, Sep. 2012, pp. 2677–2680.
[13] T. Thayaparan, L. Stankovi, and I. Djurovi, "Micro-Doppler-based target detection and feature extraction in indoor and outdoor environments," *J. Franklin Inst.*, vol. 345, no. 6, pp. 700–722, Sep. 2008.
[14] L. Stankovic, I. Djurovic, and T. Thayaparan, "Separation of target rigid body and micro-Doppler effects in ISAR imaging," *IEEE Trans. Aerosp. Electron. Syst.*, vol. 42, no. 4, pp. 1496–1506, Oct. 2006.
[15] T. Thayaparan, P. Suresh, S. Qian, K. Venkataramaniah, S. SivaSankaraSai, and K. Sridharan, "Micro-Doppler analysis of a rotating target in synthetic aperture radar," *IET Signal Process.*, vol. 4, no. 3, pp. 245–255, Jun. 2010.
[16] I. Djurovic, T. Thayaparan, and L. Stankovic, "SAR imaging of moving targets using polynomial Fourier transform," *IET Signal Process.*, vol. 2, no. 3, pp. 237–246, Sep. 2008.
[17] J. Li and H. Ling, "Application of adaptive chirplet representation for ISAR feature extraction from targets with rotating parts," *Proc. Inst. Elect. Eng.—Radar, Sonar Navig.*, vol. 150, no. 4, pp. 284–291, Aug. 2003.
[18] Q. Wang, M. Pepin, R. J. Beach, R. Dunkel, T. Atwood, B. Santhanam, W. Gerstle, and M. M. Hayat, "SAR-based vibration estimation using the discrete fractional Fourier transform," *IEEE Trans. Geosci. Remote Sens.*, vol. 50, no. 10, pp. 4145–4156, Oct. 2012.
[19] Q. Wang, M. Pepin, R. J. Beach, R. Dunkel, T. Atwood, A. W. Doerry, B. Santhanam, W. Gerstle, and M. M. Hayat, "Demonstration of target vibration estimation in synthetic aperture radar imagery," in *Proc. IEEE IGARSS*, Vancouver, BC, Canada, Aug. 2011, pp. 4083–4086.
[20] Q. Wang, M. Pepin, B. Santhanam, T. Atwood, and M. M. Hayat, "SAR-based vibration retrieval using the fractional Fourier transform in slow time," in *Proc. SPIE, Radar Sensor Technol.*, Orlando, FL, USA, Apr. 2010, vol. 7669, pp. 766 911-1–766 911-10.
[21] S. I. Tsunoda, F. Pace, J. Stence, M. Woodring, W. H. Hensley, A. W. Doerry, and B. C. Walker, "Lynx: A high-resolution synthetic aperture radar," in *Proc. SPIE, Radar Sensor Technol. IV*, 1999, vol. 3704, pp. 1–4.
[22] M. J. Collins and J. M. Allen, "Modeling and simulation of SAR image texture," *IEEE Trans. Geosci. Remote Sens.*, vol. 47, no. 10, pp. 3530–3546, Oct. 2009.
[23] J. G. Vargas-Rubio and B. Santhanam, "The centered discrete fractional Fourier transform and linear chirp signals," in *Proc. IEEE 11th DSP Workshop*, 2004, pp. 163–167.
[24] J. G. Vargas-Rubio and B. Santhanam, "An improved spectrogram using the multiangle centered discrete fractional Fourier transform," in *Proc. IEEE ICASSP*, 2005, vol. 4, pp. 505–508.
[25] J. G. Vargas-Rubio and B. Santhanam, "On the multiangle centered discrete fractional Fourier transform," *IEEE Signal Process. Lett.*, vol. 12, no. 4, pp. 273–276, Apr. 2005.
[26] B. Santhanam and J. H. McClellan, "The discrete rotational Fourier transform," *IEEE Trans. Signal Process.*, vol. 44, no. 4, pp. 994–998, Apr. 1996.
[27] L. B. Almeida, "The fractional Fourier transform and time–frequency representations," *IEEE Trans. Signal Process.*, vol. 42, no. 11, pp. 3084–3091, Nov. 1994.
[28] V. Namias, "The fractional order Fourier transform and its applications to quantum mechanics," *J. Inst. Math Appl.*, vol. 25, no. 3, pp. 241–265, Mar. 1980.
[29] R. Saxena and K. Singh, "Fractional Fourier transform: A novel tool for signal processing," *J. Indian Inst. Sci.*, vol. 85, no. 1, pp. 11–26, Jan./Feb. 2005.
[30] W. G. Carrara, R. Goodman, and R. Majewski, *Synthetic Aperture Radar—Signal Processing and Algorithms*. Norwood, MA, USA: Artech House, 1995.

Qi Wang (S'08) received the B.Sc. degree in electrical engineering from Shanghai Jiao Tong University, Shanghai, China, in 2007. He is currently working toward the Ph.D. degree in the Department of Electrical and Computer Engineering, The University of New Mexico, Albuquerque, NM, USA.

His research interests include imaging algorithms for high-resolution SAR, detection and estimation of nonstatic targets for SAR, and nonstationary signal processing.

Matthew Pepin (M'79) received the B.S.(Hons.) degree in electrical engineering and the M.E. degree from the University of Virginia, Charlottesville, VA, USA, in 1981 and 1982, respectively, and the Ph.D. degree from the Air Force Institute of Technology, Wright-Patterson AFB, OH, USA, in 1996.

He is currently a Postdoctoral Fellow with the Electrical and Computer Engineering Department, The University of New Mexico, Albuquerque, NM, USA. His research interests include sensors, spectral estimation, array processing, and imaging algorithms.

Aleck Wright, photograph and biography not available at the time of publication.

Ralf Dunkel was born in Germany. He received the B.S., M.S., and Ph.D. degrees from Martin Luther University, Halle-Wittenberg, Germany.

He is currently the Director of the Reconnaissance Systems Group of General Atomics Aeronautical Systems, Inc., San Diego, CA, USA. His primary area of focus is airborne sensor testing and data analysis.

Tom Atwood received the Ph.D. degree in electrical and computer engineering from The University of New Mexico, Albuquerque, NM, USA, in 2009.

He is currently with Sandia National Laboratories, Albuquerque. He has more than 20 years experience in designing, building, and fielding systems (including space, airborne, and terrestrial) for radar, communications, and signals intelligence. His current research areas include software reprogrammable payloads and cognitive radio/radar.

Balu Santhanam (S'92–M'98–SM'05) received the B.S. degree in electrical engineering from Saint Louis University, Saint Louis, MO, USA, in 1992 and the M.S. and Ph.D. degrees in electrical engineering from Georgia Institute of Technology, Atlanta, GA, USA, in 1994 and 1998, respectively.

From 1998 to 1999, he was a Lecturer and a Postdoctoral Researcher with the Department of Electrical and Computer Engineering (ECE), University of California, Davis, CA, USA. In 1999, he joined the Department of ECE, The University of New Mexico (UNM), Albuquerque, NM, USA, where he is currently an Associate Professor of electrical engineering. His current research interests include discrete fractional Fourier analysis and applications, multicomponent AMFM models and demodulation, signal representations for modulated signals, and hybrid ICA-SVM systems and their application to pattern recognition problems.

Dr. Santhanam is currently the Chair of the Albuquerque Chapter of the IEEE Signal Processing and IEEE Communications Societies. He served as the Technical Area Chair for adaptive systems for the Asilomar Conference on Signals, Systems, and Computers in 2004 and on the international program committee for the IEEE International Conference on Systems, Man, and Cybernetics in 2005 and 2006. He was the recipient of the 2000 and 2005 ECE-UNM Distinguished Teacher Award.

Walter Gerstle received the Ph.D. degree in structural engineering from Cornell University, Ithaca, NY, USA.

Since 1986, he has been with The University of New Mexico, Albuquerque, NM, USA, where he is currently a Professor of civil engineering and where, recently, he has been working on the structural design of optical and radio telescopes, as well as research in structural acoustics, with groups from the Department of Electrical and Computer Engineering and the Department of Physics and Astronomy. His research interests are in computational structural engineering and computational mechanics.

Armin W. Doerry received the Ph.D. degree in electrical engineering from The University of New Mexico, Albuquerque, NM, USA.

Since 1987, he has worked in numerous aspects of synthetic aperture radar and other radar systems analysis, design, and fabrication. He is currently a Distinguished Member of the Technical Staff with the Surveillance and Reconnaissance Department, Sandia National Laboratories, Albuquerque.

Majeed M. Hayat (S'89–M'92–SM'00) was born in Kuwait in 1963. He received the B.Sc. degree (*summa cum laude*) in electrical engineering from the University of the Pacific, Stockton, CA, USA, in 1985 and the M.S. and Ph.D. degrees in electrical and computer engineering from the University of Wisconsin–Madison, Madison, WI, USA, in 1988 and 1992, respectively.

He is currently a Professor of electrical and computer engineering, the Associate Director of the Center for High Technology Materials, and the General Chair of the Optical Science and Engineering Program with The University of New Mexico, Albuquerque, NM, USA. He has authored or coauthored over 82 peer-reviewed journal articles (H-Index of 27). He is a holder of six issued patents, three of which have been licensed. His research activities cover a broad range of topics including avalanche photodiodes, signal and image processing, algorithms for spectral and radar sensing and imaging, optical communication, networked computing, and modeling interdependent networks with applications to smart grids.

Dr. Hayat is a Fellow of the Optical Society of America and The International Society for Optical Engineers (SPIE). He is currently the Chair of the Topical Committee of Photodetectors, Sensors, Systems and Imaging within the IEEE Photonics Society. He was an Associate Editor of *Optics Express* from 2004 to 2009. He was the recipient of the National Science Foundation Early Faculty Career Award in 1998 and the Chief Scientist Award for Excellence by the National Consortium for MASINT Research (Defense Intelligence Agency) in 2006.